

Measurement Matrix Design for Compressive Sensing Based MIMO Radar ¹

Yao Yu

Department of Electrical & Computer Engineering, Drexel University, Philadelphia, PA 19104

Athina P. Petropulu

Department of Electrical & Computer Engineering, Rutgers, The State University of New Jersey,
Piscataway, NJ 08854-8058

H. Vincent Poor

School of Engineering and Applied Science, Princeton University, Princeton, NJ 08544

Abstract

In colocated multiple-input multiple-output (MIMO) radar using compressive sensing (CS), a receive node compresses its received signal via a linear transformation, referred to as measurement matrix. The samples are subsequently forwarded to a fusion center, where an ℓ_1 -optimization problem is formulated and solved for target information. CS-based MIMO radar exploits the target sparsity in the angle-Doppler-range space and thus achieves the high localization performance of traditional MIMO radar but with many fewer measurements. The measurement matrix is vital for CS recovery performance. This paper considers the design of measurement matrices that achieve an optimality criterion that depends on the coherence of the sensing matrix (CSM) and/or signal-to-interference ratio (SIR). The first approach minimizes a performance penalty that is a linear combination of CSM and the inverse SIR. The second one imposes a structure on the measurement matrix and determines the parameters involved so that the SIR is enhanced. Depending on the transmit waveforms, the second approach can significantly improve SIR, while maintaining CSM comparable to that of the Gaussian random measurement matrix (GRMM). Simulations indicate that the proposed measurement matrices can improve detection accuracy as compared to a GRMM.

Keywords: Compressive sensing, MIMO radar, measurement matrix, DOA estimation

I. INTRODUCTION

Multiple-input multiple-output (MIMO) radar has received considerable recent attention [1]-[3]. A MIMO radar consists of multiple transmit and receive antennas and is advantageous in two different

¹ This work was supported by the by the Office of Naval Research under Grants ONR-N-00014-07-1-0500 and ONR-N-00014-09-1-0342 and the National Science Foundation under Grants CNS-09-05398 and CNS-04-35052

scenarios [4]-[8], namely, widely separated antennas and colocated antennas. In the first scenario [4], the transmit antennas are located far apart from each other relative to their distance to the target. The MIMO radar system transmits independent probing signals from its antennas that follow independent paths, and thus each target return carries independent information about the target. Joint processing of the target returns results in diversity gain, which enables the MIMO radar to achieve high target resolution. Widely distributed MIMO radar systems are shown to offer considerable advantages for estimation of target parameters, such as location [5] and velocity [6]. In the colocated scenario [7][8], the transmit and receive antennas are located close to each other relative to the target, so that all antennas view the same aspect of the target. In this scenario, the phase differences induced by transmit and receive antennas can be exploited to form a long virtual array with the number of elements equal to the product of the numbers of transmit and receive nodes. This enables the MIMO radar to achieve superior resolution in terms of direction of arrival (DOA) estimation and parameter identification [7].

Compressive sensing (CS) theory [9]-[12] states that a signal \mathbf{x} that exhibits sparsity in some domain, can be recovered from a number of samples that is much smaller than that required by Nyquist theory. In particular, a signal of length N that can be represented by K ($K \ll N$) basis vectors in some space, can be recovered exactly with high probability from $O(K \log N)$ measurements. Let Ψ denote the basis matrix that spans that space, and Φ denote an $M \times N$ matrix with $M \ll N$, that is incoherent with Ψ and is referred to as the measurement matrix. The recovery proceeds by finding the coefficients of the K basis vectors in the signal decomposition. This is formulated as an ℓ_1 -optimization problem, i.e., $\min \|\mathbf{s}\|_1$, s.t. to $\mathbf{y} = \Phi \mathbf{x} = \Phi \Psi \mathbf{s}$. Throughout this paper, we will refer to recovery along these lines as the *CS approach*. The product $\Phi \Psi$ is usually referred to as the *sensing matrix*. According to the uniform uncertainty principle (UUP) [11]-[13], if every set of sensing matrix columns with cardinality less than the sparsity of the signal of interest is approximately orthogonal, then the sparse signal can be exactly recovered with high probability. In other words, CS recovery requires that Φ is incoherent with Ψ . For an orthonormal basis matrix, use of a random measurement matrix leads to a sensing matrix that obeys the UUP with overwhelming probability [10]. The entries of such a measurement matrix can be taken from a Gaussian distribution or symmetric Bernoulli distribution. The rows of a Fourier matrix or an orthonormal matrix could also compose a measurement matrix. In this paper, we term as *the conventional approach* CS recovery using a Gaussian measurement matrix.

The application of CS to radar and MIMO radar has been explored in [14]-[17] and [18]-[21], respectively. In both [19] and [20], the authors considered a uniform linear array as a transmit and receive antenna configuration and proposed to use a submatrix of the identity matrix as the measurement matrix.

In [18] and [21], a CS-based MIMO radar system implemented on a small scale network was proposed. The network consists of a number of transmit and receive nodes, each equipped with a single antenna, that are randomly distributed over a small area. Each transmit node transmits a different narrowband signal. If the number of targets is small, the signal that is reflected by targets and is picked up at a receive node is sparse in the angle-range-Doppler space. This fact can be exploited to achieve target detection and localization using only a small number of compressively obtained samples at each receive node, and/or by involving a small number of receive nodes [21]. The approach of [18] and [21] was applied to the case in which the targets are located within a small range bin and the sampling is synchronized with the first target return. To improve performance in the presence of strong interference the columns of the sensing matrix were designed to incorporate information on the transmit waveforms.

In this paper, we consider a general scenario that does not confine the targets within a small range bin, nor does it require sampling synchronization. When the targets are separated by several range bins, different targets will introduce different delays in the received waveforms. In that case, the formulation of [18] and [21] no longer applies. This problem was considered in [22], where a step-frequency approach was proposed in order to improve range resolution. Here, our goal is optimal or suboptimal measurement matrix design that decreases the coherence of the sensing matrix (CSM) and/or enhances signal-to-interference ratio (SIR). The first design minimizes a performance penalty that is a linear combination of CSM and the inverse SIR. The measurement matrix is obtained by solving a convex optimization problem that involves high computational complexity. A suboptimal solution is also proposed that forces a specific structure to the measurement matrix. The second design targets only SIR improvement; it is constructed based on the transmit signal waveforms and accounts for all possible discretized delays of target returns within a given time window. It is shown that depending on the waveforms used, the latter measurement matrix can significantly improve SIR while it results in CSM comparable to that of the random Gaussian measurement matrix.

The rest of the paper is organized as follows. In Section II we provide the signal model of a CS-based MIMO radar system with targets falling in different range bins. In Section III, we introduce the two proposed measurement matrices and provide the SIR analysis related to the second measurement matrix. Simulation results are given in Section IV for stationary targets. Finally, we make some concluding remarks in Section V.

Notation: Lower case and capital letters in bold denote respectively vectors and matrices. The expectation of a random variable is denoted by $E\{\cdot\}$. Superscripts $(\cdot)^H$ and $\text{Tr}(\cdot)$ denote respectively the Hermitian transpose and trace of a matrix. $A(m, n)$ represents the (m, n) -th entry of the matrix \mathbf{A} . $\mathbf{0}_{L \times M}$ denotes an

$L \times M$ matrix with zero entries.

II. SIGNAL MODEL FOR CS-BASED MIMO RADAR

Let us consider a MIMO radar system consisting of M_t transmit antennas (TXs) and N_r receive antennas (RXs) that are randomly distributed over a small area (colocated). Each TX node transmits periodic narrowband pulses of duration T_p and pulse repetition interval (PRI) T . Let $(r_i^t, \alpha_i^t)/(r_i^r, \alpha_i^r)$ denote the location of the i -th transmit/receive node in polar coordinates. Let us also consider the presence of K slowly-moving point targets located in different range bins; the k -th target is at azimuth angle θ_k and moves with constant radial speed v_k .

Let $d_k(t)$ denote the range of the k -th target at time t . Under the far-field assumption, i.e., $d_k(t) \gg r_i^{t/r}$, the distance between the i th transmit/receive node and the k -th target d_{ik}^t/d_{ik}^r can be approximated as

$$d_{ik}^{t/r}(t) \approx d_k(t) - \eta_i^{t/r}(\theta_k) = d_k(0) - \eta_i^{t/r}(\theta_k) - v_k t \quad (1)$$

where $\eta_i^{t/r}(\theta_k) = r_i^{t/r} \cos(\theta_k - \alpha_i^{t/r})$. Let us consider the return from the k -th target arriving at the l -th antenna during the m -th pulse, i.e.,

$$y_{lm}^k(t) = \sum_{i=1}^{M_t} \beta_k x_i(t - (d_{ik}^t(t) + d_{ik}^r(t))/c) \exp(j2\pi f(t - (d_{ik}^t(t) + d_{ik}^r(t))/c)) \quad (2)$$

where c , f and β_k denotes the speed of light, the carrier frequency, and the reflection coefficient of the k -th target, respectively; $x_i(t)$ represents the transmit waveform of the i -th node. Under the narrowband assumption, and due to the slow target speed so that the Doppler shift is negligible, the baseband signal corresponding to (2) becomes

$$y_{lm}^k(t) \approx \sum_{i=1}^{M_t} \beta_k x_i(t - 2d_k(0)/c) \exp(-j2\pi f(d_{ik}^t(t) + d_{ik}^r(t))/c). \quad (3)$$

Due to the closeness of the transmit and receive nodes, the distances between nodes and the target are approximately the same for all receivers. Thus, the time delay in the waveforms, induced by the k -th target can be approximately based on the range corresponding to the initial sampling time, i.e., $d_k(0)$, which is independent of the RX index. The l -th node compressively samples the return signal to obtain M samples per pulse (please refer to Fig. 1 of [21] for a schematic of the receiver). Let L denote the number of T_p/L -spaced samples of the transmitted waveforms within one pulse. The effect of the compressive receiver of Fig. 1 of [21] is equivalent to pre-multiplying by matrix Φ_l a T_p/L -sampled version of the received pulse. The size of Φ_l is $M \times (L + \tilde{L})$, where \tilde{L} is the maximum delay among the return signals

normalized by T_p/L and is known in advance. Here $M \ll L$. The obtained samples are then placed in vector \mathbf{r}_{lm} , which can be expressed in matrix form as [22]

$$\mathbf{r}_{lm} = \sum_{k=1}^K \beta_k e^{j2\pi p_{lmk}} \Phi_l \mathbf{D}(f_k) \mathbf{C}_{\tau_k} \mathbf{X} \mathbf{v}(\theta_k) + \Phi_l \mathbf{n}_{lm} \quad (4)$$

where

- 1) $p_{lmk} = \frac{-2d_k(0)f}{c} + \frac{\eta'_l(\theta_k)f}{c} + f_k(m-1)T$, where $f_k = \frac{2v_k f}{c}$ is the Doppler shift induced by the k -th target; \mathbf{X} is an $L \times M_t$ matrix that contains the transmit waveforms of M_t antennas as its columns and $\text{diag}\{\mathbf{X}^H \mathbf{X}\} = [1, \dots, 1]^T$;
- 2) Φ_l is the $M \times (L + \tilde{L})$ measurement matrix for the l -th receive node;
- 3) $\mathbf{v}(\theta_k) = [e^{j\frac{2\pi f}{c}\eta'_1(\theta_k)}, \dots, e^{j\frac{2\pi f}{c}\eta'_{M_t}(\theta_k)}]^T$ and $\mathbf{D}(f_k) = \text{diag}\{[e^{j2\pi f_k 0 T_p/L}, \dots, e^{j2\pi f_k (L+\tilde{L}-1)T_p/L}]\}$;
- 4) $\tau_k = \lfloor \frac{2d_k(0)}{cT_p/L} \rfloor$ and $\mathbf{C}_{\tau_k} = [\mathbf{0}_{L \times \tau_k}, \mathbf{I}_L, \mathbf{0}_{L \times (\tilde{L}-\tau_k)}]^T$. Here, we assume that the target returns completely fall within the sampling window of length $(L + \tilde{L})T_p/L$, and that T_p/L is small enough so that the rounding error in the delay is small, i.e., $x_i(t - \tau_k) \approx x_i(t - \frac{2d_k(0)}{cT_p/L})$.
- 5) \mathbf{n}_{lm} is the interference of variance σ^2 at the l -th receiver during the m -th pulse, arising due to the jammer signals and thermal noise.

Discretize the angle, speed and range space on a fine grid, i.e., respectively, $[\tilde{a}_1, \dots, \tilde{a}_{N_a}]$, $[\tilde{b}_1, \dots, \tilde{b}_{N_b}]$ and $[\tilde{c}_1, \dots, \tilde{c}_{N_c}]$. Let the grid points be arranged first angle-wise, then range-wise, and finally speed-wise to yield the grid points (a_n, b_n, c_n) , $n = 1, \dots, N_a N_b N_c$. Through this ordering, the grid point $(\tilde{a}_{n_a}, \tilde{b}_{n_b}, \tilde{c}_{n_c})$ is mapped to point (a_n, b_n, c_n) with $n = (n_b - 1)n_a n_c + (n_c - 1)n_a + n_a$. The discretized step is small enough so that each target falls on some angle-speed-range grid point. Then (4) can be rewritten as

$$\mathbf{r}_{lm} = \Phi_l \left(\sum_{n=1}^N s_n e^{j2\pi q_{lmn}} \mathbf{D}\left(\frac{2b_n f}{c}\right) \mathbf{C}_{\lfloor \frac{2c_n}{cT_p/L} \rfloor} \mathbf{X} \mathbf{v}(a_n) + \mathbf{n}_{lm} \right) \quad (5)$$

where $N = N_a N_b N_c$, $s_n = \begin{cases} \beta_k, & \text{if the } k\text{-th target is at } (a_n, b_n, c_n) \\ 0, & \text{otherwise} \end{cases}$ and

$$q_{lmn} = \frac{-2c_n f}{c} + \frac{\eta'_l(a_n) f}{c} + \frac{2b_n f(m-1)T}{c}. \quad (6)$$

In matrix form we have $\mathbf{r}_{lm} = \Theta_{lm} \mathbf{s} + \Phi_l \mathbf{n}_{lm}$, where $\mathbf{s} = [s_1, \dots, s_N]^T$ and

$$\Theta_{lm} = \Phi_l \underbrace{[e^{j2\pi q_{lm1}} \mathbf{D}(2b_1 f/c) \mathbf{C}_{\lfloor \frac{2c_1}{cT_p/L} \rfloor} \mathbf{X} \mathbf{v}(a_1), \dots, e^{j2\pi q_{lmN}} \mathbf{D}(2b_N f/c) \mathbf{C}_{\lfloor \frac{2c_N}{cT_p/L} \rfloor} \mathbf{X} \mathbf{v}(a_N)]}_{\Psi_{lm}}. \quad (7)$$

According to the CS formulation, Θ_{lm} is the sensing matrix and Ψ_{lm} is the basis matrix.

If the number of targets is small as compared to N , then the positions of the targets are sparse in the angle-speed-range space and \mathbf{s} is a sparse vector. The locations of the non-zero elements of \mathbf{s} provide information on target angle, speed and range. All the receive nodes forward their compressed measurements to a fusion center. We assume that the fusion center has the ability to separate the data of different nodes from each other. This can be done, for instance, if the nodes send their data over different carriers. The fusion center combines the compressively sampled signals due to N_p pulses obtained at N_r receive nodes to form the vector \mathbf{r} . Using the predefined measurement matrices, the discretization of the angle-speed-range space, and also knowledge of the waveform matrix \mathbf{X} , the fusion center obtains an estimate of \mathbf{s} by applying the Dantzig selector [23].

III. MEASUREMENT MATRIX DESIGN

In this section, we discuss the design of the measurement matrix in order to improve the detection performance of CS-MIMO radar. For the sake of simplicity, we assume that all the nodes use the same measurement matrix, denoted by Φ , which does not vary with time. Since the targets are moving slowly, the Doppler shift within a pulse can be ignored. Generally, there are two factors that affect the performance of CS. The first one is the coherence of the sensing matrix. UUP requires low CSM to guarantee exact recovery of the sparse signal. The second factor is SIR. If the basis matrix obeys the UUP and the signal of interest \mathbf{s} is sufficiently sparse, then the square estimation error of the Dantzig selector satisfies with very high probability [23]

$$\|\hat{\mathbf{s}} - \mathbf{s}\|_{\ell_2}^2 \leq C^2 2 \log N \times \left(\sigma^2 + \sum_i^N \min(s^2(i), \sigma^2) \right) \quad (8)$$

where C is a constant. It can be easily seen from (8) that an increase in the interference power degrades the performance of the Dantzig selector.

A. Measurement matrix design #1

The goal of measurement matrix design is to reduce the coherence of the sensing matrix and at the same time increase SIR. The coherence of two columns of the sensing matrix, Θ , corresponding to the

k -th and k' -th grid point is given by

$$\begin{aligned}\mu_{kk'}(\Theta) &= \frac{\left| \sum_{m=1}^{N_p} \sum_{l=1}^{N_r} e^{j2\pi(q_{lmk}-q_{lmk'})} \left(\Phi \mathbf{C}_{\lfloor \frac{2c_k}{cT_p/L} \rfloor} \mathbf{X}\mathbf{v}(a_{k'}) \right)^H \Phi \mathbf{C}_{\lfloor \frac{2c_{k'}}{cT_p/L} \rfloor} \mathbf{X}\mathbf{v}(a_k) \right|}{N_r \sqrt{\sum_{m=1}^{N_p} \left\| \Phi \mathbf{C}_{\lfloor \frac{2c_k}{cT_p/L} \rfloor} \mathbf{X}\mathbf{v}(a_k) \right\|_2^2 \sum_{m=1}^{N_p} \left\| \Phi \mathbf{C}_{\lfloor \frac{2c_{k'}}{cT_p/L} \rfloor} \mathbf{X}\mathbf{v}(a_{k'}) \right\|_2^2}} \\ &= \frac{\left| \sum_{m=1}^{N_p} \sum_{l=1}^{N_r} e^{j2\pi(q_{lmk}-q_{lmk'})} \mathbf{u}_{k'}^H \Phi^H \Phi \mathbf{u}_k \right|}{N_r N_p \sqrt{\mathbf{u}_k^H \Phi^H \Phi \mathbf{u}_k \mathbf{u}_{k'}^H \Phi^H \Phi \mathbf{u}_{k'}}}\end{aligned}\quad (9)$$

where $\mathbf{u}_k = \mathbf{C}_{\lfloor \frac{2c_k}{cT_p/L} \rfloor} \mathbf{X}\mathbf{v}(a_k)$.

Let the interference waveform at the l -th receive node during the m -th pulse be Gaussian distributed, i.e., $n_{lm}(t) \sim \mathcal{CN}(0, \sigma^2)$. Let us also assume that the noise waveforms are independent across receive nodes and between pulses. Then the average power of the interference equals

$$P_n = E \left\{ \sum_{m=1}^{N_p} \sum_{l=1}^{N_r} (\Phi \mathbf{n}_{lm})^H \Phi \mathbf{n}_{lm} \right\} = N_p N_r \sigma^2 \text{Tr}\{\Phi^H \Phi\}.\quad (10)$$

The average power of the echo reflected by the i -th target located on the k_i -th grid point of the angle-range space is approximately equal to

$$P_s^i \approx |\beta_i|^2 N_r N_p \mathbf{u}_{k_i}^H \Phi^H \Phi \mathbf{u}_{k_i}.\quad (11)$$

Therefore, the SIR equals approximately

$$\text{SIR} \approx \frac{\sum_{i=1}^K |\beta_i|^2 \mathbf{u}_{k_i}^H \Phi^H \Phi \mathbf{u}_{k_i}}{\sigma^2 \text{Tr}\{\Phi^H \Phi\}}.\quad (12)$$

The precise manner in which CSM and SIR affect the performance of the CS approach is unknown. Although theoretical bounds for the ℓ_2 -norm of the estimation error have been proposed [23]-[25], those bounds might not be relevant in applications in which the quantities of interests are the locations of the non-zero elements of the sparse signal, rather than the non-zero values themselves. This is the case in the problem at hand. In [26], an upper bound on the error probability of sparse support recovery, i.e., the total probability of missed detection and false alarm, under the optimal decision rule was derived. Although that upper bound is related to the detection of non-zero elements, it cannot be used for the design of the measurement matrix because it is rather loose, and further, it involves eigenvalues of submatrices of a given sensing matrix corresponding to all possible sparse patterns for the signal of interest.

In this paper, we determine the measurement matrix by optimizing a linear combination of CSM and

the reciprocal of SIR. The CSM can be defined in various ways. Let us define CSM as the maximum coherence produced by a pair of cross columns in the sensing matrix. This criterion works well for a uniform sensing matrix but might not capture the behavior of the sensing matrix in cases in which the coherence of most column pairs is small [27]. However, this coherence metric is widely used for the CS scenario due to its simplicity [27][28].

The optimization problem becomes

$$\min_{\Phi} \left(\max_{k \neq k'} \mu_{kk'}^2(\Phi) + \lambda \frac{1}{\text{SIR}} \right) \quad (13)$$

where λ is a positive weight, which reflects the tradeoff between the CSM and SIR.

The problem of (12) is not convex. In order to obtain a solution, let us first view (12) as an optimization problem with respect to $\mathbf{B} = \Phi^H \Phi$. Furthermore, let us set the norm of the columns of the sensing matrix to 1, i.e., $N_r N_p \mathbf{u}_k^H \Phi^H \Phi \mathbf{u}_k = 1$, $k = 1, \dots, N$; this will significantly simplify the expression for $\mu_{kk'}(\Phi)$ and $\frac{1}{\text{SIR}}$. Now, (12) can be reformulated (using the approximation (12)) as

$$\begin{aligned} \min_{t, \mathbf{B}} \quad & t + \lambda \text{Tr}\{\mathbf{B}\} \\ \text{s.t.} \quad & \left| \sum_{m=1}^{N_p} \sum_{l=1}^{N_r} e^{j2\pi(q_{lmk'} - q_{lmk})} \mathbf{u}_{k'}^H \mathbf{B} \mathbf{u}_k \right|^2 \leq t, \\ & k = 1, \dots, N, k' = k + 1, \dots, N \\ & N_r N_p \mathbf{u}_k^H \mathbf{B} \mathbf{u}_k = 1, \quad k = 1, \dots, N, \\ & \mathbf{B} \geq 0, \quad t \geq 0, \end{aligned} \quad (14)$$

which is a convex problem with respect to \mathbf{B} . The first term in the objective refers to the maximum coherence of cross columns in the sensing matrix; the second term is proportional to the noise power which is a linear function of \mathbf{B} . Once \mathbf{B} is obtained, the solution of (12) can be obtained based on the eigendecomposition $\mathbf{B} = \mathbf{V} \Sigma \mathbf{V}^H$, as

$$\Phi_{\#1} = \sqrt{\tilde{\Sigma}} \tilde{\mathbf{V}}^H \quad (15)$$

where $\tilde{\Sigma}$ is a diagonal matrix that contains on its diagonal the nonzero eigenvalues of Σ , and $\tilde{\mathbf{V}}$ contains as its columns the corresponding eigenvectors.

Another definition for CSM would be as the sum of the coherence of all pairs of columns in the

sensing matrix (SCSM). With this measure of CSM, the minimization problem becomes

$$\min_{\Phi} \left(\sum_{k \neq k'} \mu_{kk'}^2(\Theta) + \lambda \frac{1}{\text{SIR}} \right). \quad (16)$$

Simulation results show that the solution of (16) can increase the number of column pairs in the sensing matrix that have low coherence as compared to the solution of (14). The latter solution tends to increase the coherence of some column pairs in the sensing matrix which had low coherence. This is intuitively expected because solving (14) requires more constraints than (16). In this paper, we use SCSM to design the measurement matrix.

The above proposed methods for optimizing the measurement matrix reduce the coherence of cross columns in the sensing matrix without amplifying the interference. These methods improve the detection performance of the CS-based MIMO radar system, but incur an increased computational load as compared to CS-based MIMO radar that relies on the conventional measurement matrix. The number of complex variables entering the convex problem of (16) is $\frac{(\tilde{L}+L+1)(\tilde{L}+L)}{2}$. The computation complexity would be prohibitively high for large values of $\tilde{L} + L$. Also, for a large number of grid points N , we have to deal with a large number of constraints. The optimal measurement matrix might be obtained and stored offline based on knowledge of grid points in the angle-range space. However, it would need to be updated once the basis matrix changes with the search area of interest. This would bring heavy burden to radar systems and thus might render the real-time application impossible. Therefore, ways to alleviate the computational load are worthy of investigation. A suboptimal scheme for this problem that involves lower complexity is discussed next.

Let us impose a structure on the measurement matrix to be determined as follows:

$$\Phi_{\#1} = \mathbf{W}\Phi \quad (17)$$

where \mathbf{W} is an $(L + \tilde{L}) \times \tilde{M}$ unknown matrix to be determined and Φ is a $\tilde{M} \times M_r(\tilde{L} + 1)$ Gaussian random matrix. Then the number of variables in \mathbf{W} can be controlled by changing the value of \tilde{M} . We can obtain \mathbf{W} by solving (16) with $\mathbf{B} = \mathbf{W}^H \mathbf{W}$ and $\mathbf{u}_k = \Phi \mathbf{C}_{\lfloor \frac{2c_k}{cT_p/L} \rfloor} \mathbf{X} \mathbf{v}(a_k)$. Furthermore, the structure in (17) enables a two-step processing for CS-based MIMO radar that simplifies the hardware of the receive nodes. In particular, a receive node linearly compresses the incident signal by using Φ . At the fusion center, all the signals forwarded by receive nodes are first multiplied by \mathbf{W} and then jointly processed to extract target information. We can think of \mathbf{W} as a type of post processing. In this way, the received nodes require no information about \mathbf{W} , which reduces the communication overhead for the fusion center and nodes.

In order to render the convex problem tractable, the norm of the columns in the sensing matrix is set to be a constant. This increases the number of constraints. If the number of variables is not sufficiently high, there might not be enough degrees of freedoms to decrease the coherence of the sensing matrix as compared to the original one. Since the number of constraints equals the number of grid points, the number of constraints can be decreased by reducing the search area. This can be done by considering grid points around some initial angle-range estimates, if such estimates are available.

B. Measurement matrix design #2

Although the suboptimal construction in (17) significantly reduces the number of variables, solving (16) still requires high computational load. Further, the solution needs to be adapted to a particular basis matrix. In order to avoid these two shortcomings of $\Phi_{\#1}$, we next propose another measurement matrix that targets SIR improvement only.

As in [21], we impose a special structure on the measurement matrix, i.e.,

$$\Phi_{\#2} = \Phi \mathbf{W}^H, \quad (18)$$

where Φ is an $M \times \tilde{M}$ ($M \leq \tilde{M}$) zero-mean Gaussian random matrix and \mathbf{W} is an $(L + \tilde{L}) \times \tilde{M}$ deterministic matrix satisfying $\text{diag}\{\mathbf{W}^H \mathbf{W}\} = [1, \dots, 1]^T$. The above structure serves two purposes. First, the matrix \mathbf{W} can be selected to improve the detection performance of the CS approach at the receiver. Second, $\Phi_{\#2}$ is always Gaussian regardless of \mathbf{W} . As will be shown next, with the appropriate \mathbf{W} , $\Phi_{\#2}$ may not result in higher CSM as compared to the conventional measurement matrix. Next, we discuss the selection of \mathbf{W} .

The average power of the echo reflected by the k -th target with respect to node locations, conditioned on the transmit waveforms, is approximately equal to

$$\begin{aligned} P_s^k &\approx |\beta_k|^2 N_r N_p E\{\text{Tr}\{\Phi \mathbf{W}^H \mathbf{C}_{\tau_k} \mathbf{X} \mathbf{v}(\theta_k) (\Phi \mathbf{W}^H \mathbf{C}_{\tau_k} \mathbf{X} \mathbf{v}(\theta_k))^H\}\} \\ &\approx |\beta_k|^2 N_r N_p \text{Tr}\{\Phi \mathbf{W}^H \mathbf{C}_{\tau_k} \mathbf{X} E\{\mathbf{V}_k\} \mathbf{X}^H \mathbf{C}_{\tau_k}^H \mathbf{W} \Phi^H\} \end{aligned} \quad (19)$$

where $\mathbf{V}_k = \mathbf{v}(\theta_k) \mathbf{v}^H(\theta_k)$ and its (i, j) -th entry can be expressed as $V_k(i, j) = e^{j \frac{2\pi f}{c} (r_i^t \cos(\theta_k - \alpha_i) - r_j^t \cos(\theta_k - \alpha_j))}$. As already noted, the Doppler shift within a pulse is ignored in (19). Since the nodes are uniformly dispersed on a disk of radius r , the distribution of $h \triangleq \frac{r_i^{t/r}}{r} \sin(\alpha_i^{t/r} - \psi_0)$ is given by [29]

$$f_h(h) = \frac{2}{\pi} \sqrt{1 - h^2}, -1 < h < 1 \quad (20)$$

so that

$$E \{ e^{j\alpha h} \} = 2 \frac{J_1(\alpha)}{\alpha} \quad (21)$$

where $J_1(\cdot)$ is the first-order Bessel function of the first kind. Thus, based on (21) we can obtain [21]

$$\begin{aligned} & E \left\{ e^{j \frac{2\pi f}{c} (r_i^t \cos(\theta_k - \alpha_i) - r_j^t \cos(\theta_{k'} - \alpha_j))} \right\} \\ &= \begin{cases} 1 & i = j \text{ and } k = k' \\ \varsigma(4 \sin(\frac{\theta_{k'} - \theta_k}{2})) & i = j \text{ and } k \neq k' \\ \varsigma^2(2) & i \neq j \end{cases} \end{aligned} \quad (22)$$

where $\varsigma(x) = 2 \frac{J_1(x \frac{\pi r f}{c})}{x \frac{\pi r f}{c}}$. As observed in [21], the terms multiplied by $\varsigma^2(2)$ are small enough and can be neglected. Thus, the average power P_s^k in (19) can be further approximated by

$$\begin{aligned} P_s^k &\approx |\beta_k|^2 N_p N_r \text{Tr}\{\mathbf{\Phi} \mathbf{W}^H \mathbf{C}_{\tau_k} \mathbf{X} \mathbf{X}^H \mathbf{C}_{\tau_k}^H \mathbf{W} \mathbf{\Phi}^H\} \\ &\approx \frac{|\beta_k|^2 M N_p N_r}{\tilde{M}} \text{Tr}\{\mathbf{W}^H \mathbf{C}_{\tau_k} \mathbf{X} \mathbf{X}^H \mathbf{C}_{\tau_k}^H \mathbf{W}\}. \end{aligned} \quad (23)$$

Inserting $\mathbf{\Phi}_{\#2}$ into (10), the average power of the interference can be approximated as

$$P_n = \sigma^2 N_p N_r \text{Tr}\{\mathbf{\Phi} \mathbf{W}^H \mathbf{W} \mathbf{\Phi}^H\} = \sigma^2 N_p N_r \sum_{q=1}^M \sum_{i,j} \Phi_{qi} w_{ij} \Phi_{qj}^* \approx \sigma^2 N_p N_r M \quad (24)$$

where Φ_{ij} and w_{ij} are the (i, j) -th entries of $\mathbf{\Phi}$ and $\mathbf{W}^H \mathbf{W}$, respectively. The approximation in (24) uses the constraint $\text{diag}\{\mathbf{W}^H \mathbf{W}\} = [1, \dots, 1]^T$ and the fact that $\sum_{q=1}^M \sum_{i \neq j} \Phi_{qi} w_{ij} \Phi_{qj}^* \approx 0$ for sufficiently large \tilde{M} due to $\Phi_{qi} \sim \mathcal{N}(0, 1/\tilde{M})$.

Based on (23) and (24), the SIR is given approximately by

$$SIR_k = P_s^k / P_n \approx \frac{|\beta_k|^2}{\sigma^2 \tilde{M}} \text{Tr}\{\mathbf{W}^H \mathbf{Q}_{\tau_k} \mathbf{W}\} \quad (25)$$

where $\mathbf{Q}_{\tau_k} = \mathbf{C}_{\tau_k} \mathbf{X} \mathbf{X}^H \mathbf{C}_{\tau_k}^H$ is an $(L + \tilde{L}) \times (L + \tilde{L})$ matrix of rank M_t . The maximization of SIR_k over \mathbf{W} can thus be approximated by the problem

$$\begin{aligned} \mathbf{W}^* &= \max_{\mathbf{W}, \tilde{M}} \frac{|\beta_k|^2}{\sigma^2 \tilde{M}} \text{Tr}\{\mathbf{W}^H \mathbf{Q}_{\tau_k} \mathbf{W}\} \\ &\text{s.t. } \text{diag}\{\mathbf{W}^H \mathbf{W}\} = [1, \dots, 1]_{\tilde{M} \times 1}^T. \end{aligned} \quad (26)$$

It can be easily seen that \mathbf{W}^* contains as its columns the eigenvectors corresponding to the largest

eigenvalue of \mathbf{Q}_{τ_k} . Since the largest eigenvalue of \mathbf{Q}_{τ_k} is not greater than $\text{Tr}\{\mathbf{Q}_{\tau_k}\} = M_t$, the maximum SIR_k is bounded by

$$\text{Bound 1 : } \frac{|\beta_k|^2}{\sigma^2} \leq SIR_k \leq \frac{|\beta_k|^2 M_t}{\sigma^2}. \quad (27)$$

The upper bound is achieved when the rank of \mathbf{X} equals 1, i.e., all the transmit nodes send out the same waveforms. When orthogonal waveforms are utilized, i.e., $\mathbf{X}^H \mathbf{X} = \mathbf{I}_{M_t}$, the SIR_k reaches the lower bound.

It can be shown that, when the transmit waveform are orthogonal, i.e., $\mathbf{X}^H \mathbf{X} = \mathbf{I}_{M_t}$, \mathbf{Q}_{τ_k} has M_t nonzero eigenvalues which are all equal to 1. Therefore, for a fixed \tilde{M} , $\tilde{M} \leq M_t$, the optimal \mathbf{W} contains the \tilde{M} eigenvectors of \mathbf{Q}_k corresponding to eigenvalue 1 and achieves maximum SIR_k equal to $SIR_k = \frac{|\beta_k|^2}{\sigma^2}$. Since the maximum SIR_k is independent of \tilde{M} , any matrix containing \tilde{M} , $\tilde{M} \leq M_t$, eigenvectors of \mathbf{Q} corresponding to eigenvalue 1 would give rise to the maximum SIR_k . However, $\tilde{M} = M_t$ results in smaller CSM than any \tilde{M} less than M_t due to the fact that the rank of \mathbf{W} is \tilde{M} . Therefore, the optimal \mathbf{W} is

$$\mathbf{W}^{**} = \mathbf{C}_{\tau_k} \mathbf{X}. \quad (28)$$

For the case of completely coherent transmit waveforms in which the upper bound in (27) is achieved, the resulting \mathbf{W}^{**} is rank deficient.

Unfortunately, \mathbf{W}^{**} is not achievable since it depends on the time delay induced by a target, τ_k , which is unknown. To address this issue, we replace SIR_k in the objective function in (26) with the average SIR_k , where the average is taken over all possible delays, and is denoted here by $\overline{SIR_k}$. Assuming that the time delay induced by the k -th target follows a discrete uniform distribution, i.e., $p(\tau_k = k) = \frac{1}{\tilde{L}+1}$, $k = 0, \dots, \tilde{L}$, we can write

$$\overline{SIR_k} = \frac{|\beta_k|^2}{\sigma^2 \tilde{M}} \sum_{\tau=0}^{\tilde{L}} \frac{1}{\tilde{L}+1} \text{Tr}\{\mathbf{W}^H \mathbf{Q}_{\tau} \mathbf{W}\} = \frac{|\beta_k|^2}{\sigma^2 \tilde{M}} \frac{1}{\tilde{L}+1} \text{Tr}\{\mathbf{W}^H \mathbf{C} \mathbf{W}\} \quad (29)$$

where

$$\mathbf{C} = \sum_{\tau=0}^{\tilde{L}} \mathbf{Q}_{\tau} = [\mathbf{C}_0 \mathbf{X}, \dots, \mathbf{C}_{\tilde{L}} \mathbf{X}] [\mathbf{C}_0 \mathbf{X}, \dots, \mathbf{C}_{\tilde{L}} \mathbf{X}]^H. \quad (30)$$

Therefore, the optimization problem that maximizes $\overline{SIR_k}$ can be rewritten as

$$\begin{aligned} \mathbf{W}^* &= \max_{\mathbf{W}, \tilde{M}} \overline{SIR_k} \\ \text{s.t. } \text{diag}\{\mathbf{W}^H \mathbf{W}\} &= [1, \dots, 1]_{\tilde{M} \times 1}^T. \end{aligned} \quad (31)$$

The solution \mathbf{W}^* of the above problem contains as its columns the eigenvectors corresponding to the largest eigenvalue of \mathbf{C} . Unlike (26), we cannot find a close-form solution to (31) that has sufficiently high rank. Further, the problem of (31) is non-convex. Inspired by the form of (28), we propose a feasible \mathbf{W} by taking all possible delays into account as follows:

$$\mathbf{W} = [\mathbf{C}_0\mathbf{X}, \dots, \mathbf{C}_{\tilde{L}}\mathbf{X}]. \quad (32)$$

Since $\mathbf{C}_i\mathbf{X}$ contains eigenvectors corresponding to the largest eigenvalues of \mathbf{Q}_i , utilizing (32) results in the average SIR_k bounded by

$$\text{Bound 2 : } \frac{|\beta_k|^2}{\sigma^2} \frac{1}{\tilde{L} + 1} + \Delta \leq \overline{SIR_k} \leq \frac{|\beta_k|^2}{\sigma^2} \frac{M_t}{\tilde{L} + 1} + \Delta \quad (33)$$

where Δ denotes $\frac{|\beta_k|^2}{\sigma^2 M_t (\tilde{L} + 1)^2} \text{Tr}\{\sum_{\tau' \neq \tau} \mathbf{X}^H \mathbf{C}_{\tau'}^H \mathbf{Q}_{\tau'} \mathbf{C}_{\tau'} \mathbf{X}\}$. One can see that *Bound 2* would be reduced to *Bound 1* when $\tilde{L} = 0$.

Next, we examine the resulting SIR based on three types of waveforms, namely a rectangular pulse, independently generated quadrature phase shift keying (QPSK) waveforms and Hadamard codes. In particular, we show that using $\Phi_{\#2}$ can suppress interference uncorrelated with the transmit waveforms, and maintains coherence as low as that corresponding to the Gaussian random measurement matrix.

1) SIR under the conventional measurement matrix: Let us consider a conventional measurement matrix Φ_c , which is an $M \times (L + \tilde{L})$ Gaussian random matrix of unit column norm with $\text{Tr}\{\Phi_c \Phi_c^H\} = M$. The average power of the interference is $P_n = \sigma^2 M$ (see (10)).

Let \mathbf{S}_i be a square matrix, formed by shifting the main diagonal of \mathbf{I}_L up by i positions. It can be easily seen that $\mathbf{S}_i^H = \mathbf{S}_{-i}$. The average power of the target returns from K targets at a receive node, conditioned on the transmit waveforms, equals

$$P_s = E\{\mathbf{r}^H \mathbf{r} | \mathbf{X}\} = \sum_k P_s^k + \sum_{k \neq k'} P_s^{k,k'} \quad (34)$$

where

$$\begin{aligned}
P_s^k &= |\beta_k|^2 E\{\text{Tr}\{\mathbf{\Phi}_c \mathbf{C}_{\tau_k} \mathbf{X} \mathbf{v}(\theta_k) (\mathbf{\Phi}_c \mathbf{C}_{\tau_k} \mathbf{X} \mathbf{v}(\theta_k))^H\}\} \\
&\approx |\beta_k|^2 \text{Tr}\{\mathbf{\Phi}_c \mathbf{C}_{\tau_k} \mathbf{X} \mathbf{X}^H \mathbf{C}_{\tau_k}^H \mathbf{\Phi}_c^H\} \\
&\approx \frac{M_t M |\beta_k|^2}{L + \tilde{L}}
\end{aligned} \tag{35}$$

and

$$P_s^{k,k'} \approx \underbrace{\beta_k^* \beta_{k'} s^2 \left(4 \sin\left(\frac{\theta_k - \theta_{k'}}{2}\right)\right)}_{\gamma_{kk'}} e^{\frac{4\pi f(d_k(0) - d_{k'}(0))}{c}} \frac{M}{L + \tilde{L}} \text{Tr}\{\mathbf{X}^H \mathbf{S}_{\tau_k - \tau_{k'}} \mathbf{X}\}. \tag{36}$$

2) *SIR for the measurement matrix $\mathbf{\Phi}_{\#2}$* : The proposed measurement matrix $\mathbf{\Phi}_{\#2} = \mathbf{\Phi} \mathbf{W}^H$ results in the same average interference power as the matrix $\mathbf{\Phi}_c$. The average power of the desired signal conditioned on the transmit waveforms, \tilde{P}_s , however, will improve. Like (34), \tilde{P}_s can be partitioned into the sum of the autocorrelation, \tilde{P}_s^k , and cross correlation, $\tilde{P}_s^{k,k'}$, of the returns from K targets. It holds that

$$\begin{aligned}
\tilde{P}_s^k &= |\beta_k|^2 E\{\text{Tr}\{\tilde{\mathbf{\Phi}}_{\#2} \mathbf{C}_{\tau_k} \mathbf{X} \mathbf{v}(\theta_k) (\tilde{\mathbf{\Phi}}_{\#2} \mathbf{C}_{\tau_k} \mathbf{X} \mathbf{v}(\theta_k))^H\}\} \\
&\approx |\beta_k|^2 \text{Tr}\{\mathbf{\Phi} \mathbf{W}^H \mathbf{C}_{\tau_k} \mathbf{X} \mathbf{X}^H \mathbf{C}_{\tau_k}^H \mathbf{W} \mathbf{\Phi}^H\} \\
&\approx \frac{|\beta_k|^2 M}{(\tilde{L} + 1) M_t} \text{Tr}\{\mathbf{W}^H \mathbf{C}_{\tau_k} \mathbf{X} \mathbf{X}^H \mathbf{C}_{\tau_k}^H \mathbf{W}\} \\
&= \frac{|\beta_k|^2 M}{(\tilde{L} + 1) M_t} \sum_{q=0}^{\tilde{L}} \text{Tr}\{\mathbf{X}^H \mathbf{S}_{q-\tau_k} \mathbf{X} \mathbf{X}^H \mathbf{S}_{q-\tau_k}^H \mathbf{X}\}
\end{aligned} \tag{37}$$

and

$$P_s^{k,k'} \approx \frac{\gamma_{kk'} M}{(\tilde{L} + 1) M_t} \sum_{q=0}^{\tilde{L}} \text{Tr}\{\mathbf{X}^H \mathbf{S}_{\tau_k - q} \mathbf{X} \mathbf{X}^H \mathbf{S}_{q - \tau_{k'}}^H \mathbf{X}\}. \tag{38}$$

For orthogonal, or randomly generated waveforms across the transmit nodes, \tilde{P}_s^k always dominates the average power of the desired signal. In order to increase \tilde{P}_s^k , the quantity $\text{Tr}\{\mathbf{X}^H \mathbf{S}_{q-\tau_k} \mathbf{X} \mathbf{X}^H \mathbf{S}_{q-\tau_k}^H \mathbf{X}\}$ in (37) needs to be as large as possible. $\mathbf{X}^H \mathbf{S}_m \mathbf{X}$ can be expressed as

$$\mathbf{X}^H \mathbf{S}_m \mathbf{X} = \begin{cases} \mathbf{X}_{1:L-m}^H \mathbf{X}_{m+1:L}, & m \geq 0 \\ \mathbf{X}_{1-m:L}^H \mathbf{X}_{1:L+m}, & \text{otherwise} \end{cases} \tag{39}$$

where $\mathbf{X}_{i:j}$ denotes the matrix that contains the rows of \mathbf{X} indexed from i to j .

Eq. (39) implies that the non-circular autocorrelation of the waveform sequence of a transmit node, i.e., $R_i(\tau) = \int_{t=0}^{T_p} x_i(t) x_i^*(t - \tau)$, $i = 1, \dots, M_t$, should be insensitive to the shift. This essentially requires a

narrowband signal. Based on this principle, the best candidate is a rectangular pulse and the maximum \tilde{P}_s equals

$$\begin{aligned}\tilde{P}_s &= \frac{MM_t}{(\tilde{L}+1)} \sum_{k=1}^K \sum_{q=0}^{\tilde{L}} |\beta_k|^2 \left(\frac{L-|q-\tau_k|}{L} \right)^2 + \frac{MM_t}{(\tilde{L}+1)} \sum_{k \neq k'}^{\tilde{L}} \sum_{q=0}^{\tilde{L}} \gamma_{kk'} \frac{(L-|\tau_k-q|)(L-|q-\tau_{k'}|)}{L^2} \\ &\leq MM_t \left(\sum_{k=1}^K |\beta_k|^2 + \sum_{k \neq k'} \gamma_{kk'} \right).\end{aligned}\quad (40)$$

The equality in (40) holds only if the targets induce identical delays and the sampling window is of a length that exactly covers the duration of target returns. Obviously, the transmit nodes cannot use identical waveforms. This is because the transmit waveforms are required to be orthogonal, or randomly generated in order to maintain low CSM.

Similarly, the minimum average power of the desired signal is achieved when randomly generated QPSK waveforms are used, because such waveforms cover the widest bandwidth for the fixed pulsed duration T_p and the length of waveforms L . The corresponding value of \tilde{P}_s is approximately

$$\tilde{P}_s \approx \frac{M}{(\tilde{L}+1)} \sum_{k=1}^K |\beta_k|^2 \left(\sum_{q=0, q \neq \tau_k}^{\tilde{L}} M_t \frac{L-|q-\tau_k|}{L^2} + 1 \right).\quad (41)$$

For orthogonal Hadamard waveforms that are of smaller bandwidth than the randomly generated QPSK waveforms, the average power of the desired signal equals approximately

$$\tilde{P}_s \approx \frac{M}{(\tilde{L}+1)} \sum_{k=1}^K \sum_{q=0}^{\tilde{L}} |\beta_k|^2 \left(\frac{L-|q-\tau_k|}{L} \right)^2.\quad (42)$$

Recall that \mathbf{W}^* corresponding to the true delay gives rise to the maximum received signal power. Adding the terms $\mathbf{C}_{\tilde{\tau}_k} \mathbf{X}$, $\tilde{\tau}_k \neq \tau_k$ to \mathbf{W} (see (32)) would lower \tilde{P}_s^k . When a coarse delay estimate is available, we need to consider only delays around that estimate and thus the length of the sampling window can be shortened. This effectively reduces the number of possible delays that are considered for the construction of \mathbf{W} . Therefore, \tilde{P}_s^k can be improved for the waveforms considered above if a coarse delay estimate is available.

3) *The SIR gain:* Let SIR_p and SIR_c denote the SIR corresponding to measurement matrices $\Phi_{\#2}$ and Φ_c , respectively. When transmitting Hadamard codes, the SIR gain induced by using the proposed

measurement matrix can be expressed as

$$\begin{aligned} r_{Ha} &= \frac{P_s}{\tilde{P}_s} \approx \frac{\frac{M}{(\tilde{L}+1)} \sum_{k=1}^K \sum_{q=0}^{\tilde{L}} |\beta_k|^2 \left(\frac{L-|q-\tau_k|}{L} \right)^2}{\sum_{k=1}^K \frac{M_t M |\beta_k|^2}{L+\tilde{L}}} \\ &= \frac{L+\tilde{L}}{M_t(\tilde{L}+1)L^2} \frac{\sum_{k=1}^K |\beta_k|^2 C_k}{\sum_{k=1}^K |\beta_k|^2} \end{aligned} \quad (43)$$

where

$$C_k = \sum_{q=0}^{\tilde{L}} (L-|q-\tau_k|)^2 = (\tilde{L}+1-2L)(\tau_k - \tilde{L}/2)^2 + \sum_{q=L-\tilde{L}}^L q^2 + \frac{(2L-\tilde{L}-1)\tilde{L}^2}{4}. \quad (44)$$

For a fixed \tilde{L} and L , with $0 \leq \tilde{L} \leq 2L-1$, C_k can be bounded as

$$\sum_{q=L-\tilde{L}}^L q^2 \leq C_k \leq \sum_{q=L-\tilde{L}}^L q^2 + \frac{(2L-\tilde{L}-1)\tilde{L}^2}{4}. \quad (45)$$

Therefore, lower and upper bounds on the approximate SIR gain using Hadamard codes are given by

$$\frac{(L+\tilde{L}) \sum_{q=L-\tilde{L}}^L q^2}{M_t(\tilde{L}+1)L^2} \leq r_{Ha} \leq \frac{(L+\tilde{L})(\sum_{q=L-\tilde{L}}^L q^2 + \frac{(2L-\tilde{L}-1)\tilde{L}^2}{4})}{M_t(\tilde{L}+1)L^2}. \quad (46)$$

Similarly, the SIR gain using randomly generated QPSK waveforms is bounded by

$$\frac{(L+\tilde{L})(\sum_{q=L-\tilde{L}}^L q + \frac{L^2}{M_t} - L)}{(\tilde{L}+1)L^2} \leq r_{QPSK} \leq \frac{(L+\tilde{L})(\sum_{q=L-\tilde{L}}^L q + \frac{\tilde{L}^2}{4} + \frac{L^2}{M_t} - L)}{(\tilde{L}+1)L^2}. \quad (47)$$

As long as $\tilde{L} < L$ and $M_t < L$, r_{QPSK} is always greater than 1. When $\frac{\sum_{q=L-\tilde{L}}^L q^2}{M_t \sum_{q=L-\tilde{L}}^L q} > 1$, the lower bound on r_{Ha} is higher than that on r_{QPSK} . For a sufficiently long L and moderate M_t , r_{Ha} would be superior to r_{QPSK} . Based on (40) and (42), one can infer that the SIR gain using the rectangular pulse is approximately M_t times greater than that using Hadamard codes.

4) *The CSM based on the suboptimal measurement matrix #2* : In this section, we examine the effect of the proposed \mathbf{W} in (32) on the CSM. For simplicity, the targets are considered to be stationary and the possible delays for constructing \mathbf{W} are based on the range grid points used to form the basis matrix. Then the sensing matrix based on $\Phi_{\#2}$, or the Gaussian random matrix can be respectively represented as

$$\Theta = \Phi_{\#2} \Psi = \Phi_{M \times (\tilde{L}+1)M_t} \mathbf{W}^H \mathbf{W} \mathbf{V} \quad (48)$$

and

$$\tilde{\Theta} = \Phi_{M \times (L+\tilde{L})} \Psi = \Phi_{M \times (L+\tilde{L})} \mathbf{W} \mathbf{V} \quad (49)$$

where $\mathbf{V} = \text{kron}(\mathbf{I}_{\tilde{L}+1}, [\mathbf{v}(a_1), \dots, \mathbf{v}(a_{N_a})])$ and $\Phi_{i \times j}$ is an $i \times j$ Gaussian random matrix whose entries are of zero mean and variance $1/j$. For sufficiently large j , the column coherence of Θ can be approximated as

$$\mu_{kk'}(\Theta) = \frac{|\sum_i (\sum_m \Phi(m, i) \Phi^*(m, i)) v_{kk'}(i)|}{\sqrt{\sum_i (\sum_m \Phi(m, i) \Phi^*(m, i)) v_{kk}(i) \sum_i (\sum_m \Phi(m, i) \Phi^*(m, i)) v_{k'k'}(i)}} \quad (50)$$

where $v_{kk'}(i)$ denotes the i -th diagonal element of the matrix $\mathbf{W}^H \mathbf{C}_{\lfloor \frac{2c_k}{cT_p/L} \rfloor} \mathbf{X} \mathbf{v}_m(a_k) \left(\mathbf{W}^H \mathbf{C}_{\lfloor \frac{2c_{k'}}{cT_p/L} \rfloor} \mathbf{X} \mathbf{v}_m(a_{k'}) \right)^H$. Without loss of generality, we let the columns of Φ be of unit norm. Then (50) can be further written as

$$\mu_{kk'}(\Theta) = \frac{|\sum_i v_{kk'}(i)|}{\sqrt{\sum_i v_{kk}(i) \sum_i v_{k'k'}(i)}}. \quad (51)$$

One can easily see from (51) that the coherence of Θ is approximately equal to that of matrix $\mathbf{W}^H \mathbf{W} \mathbf{V}$. The same conclusion applies to $\tilde{\Theta}$ as well, i.e., the coherence of $\tilde{\Theta}$ is approximately equal to that of matrix $\mathbf{W} \mathbf{V}$. Since $\mathbf{W}^H \mathbf{W}$ is more ill-conditioned than \mathbf{W} , the conditional number of $\mathbf{W}^H \mathbf{W} \mathbf{V}$ is greater than that of $\mathbf{W}^H \mathbf{W}$. Therefore, using $\Phi_{\#2}$ increases the maximum CSM as compared to the Gaussian random measurement matrix with high probability. However, for a well conditioned \mathbf{W} , the increase of the maximum CSM caused by $\Phi_{\#2}$ is negligible.

C. $\Phi_{\#1}$ v.s. $\Phi_{\#2}$

We have proposed two measurement matrices based on different performance metrics. The advantages and disadvantages of $\Phi_{\#1}$ and $\Phi_{\#2}$ are summarized as follows.

- *Complexity*

Solving $\Phi_{\#1}$ involves a complex optimization problem and depends on a particular basis matrix, while $\Phi_{\#2}$ requires knowledge only of all the possible discretized time delays. Therefore, the construction of $\Phi_{\#1}$ involves higher computational complexity than does $\Phi_{\#2}$.

- *Performance*

$\Phi_{\#1}$ aims at decreasing the coherence of the sensing matrix and enhancing SIR simultaneously. The tradeoff between CSM and SIR results in $\Phi_{\#1}$ yielding lower SIR than $\Phi_{\#2}$. Therefore, $\Phi_{\#1}$ is expected to perform better than $\Phi_{\#2}$ in the case of low interference, while it should perform worse in the presence of strong interference.

IV. SIMULATION RESULTS

In this section, we demonstrate the performance of CS-based MIMO radar when using the proposed measurement matrices $\Phi_{\#1}$ and $\Phi_{\#2}$, respectively. We consider a MIMO radar system with transmit and receive nodes uniformly located on a disk of radius 10m. The carrier frequency is $f = 5GHz$. The received signal is corrupted by zero-mean Gaussian noise. The signal-to-noise ratio (SNR) is defined as the inverse of the power of thermal noise at a receive node. A jammer is located at angle 7° and transmits an unknown Gaussian random waveform. The targets are assumed to fall on the grid points.

A. The proposed measurement matrix $\Phi_{\#2}$

1) *SIR improvement*: $M = 30$ compressed measurements are forwarded to the fusion center by each receive node. The maximum possible delay is $\tilde{L} = 100$. Figure 1 compares the numerical and theoretical SIR produced using the rectangular-pulse, Hadamard waveforms and randomly generated QPSK waveforms for the case of $M_t = 30$ transmit nodes and $N_r = 1$ receive node. The SIR performance, shown in Fig. 1, is the average of 1000 independent and random runs. The theoretical SIR of these three sequences is calculated based on (40), (42) and (41), respectively. The power of thermal noise is fixed to 1 and the power of the jammer varies from $-20dB$ to $60dB$. Applying the proposed measurement $\Phi_{\#2}$ at the receivers, the rectangular pulse and Hadamard waveforms produce a significant SIR gain over the Gaussian random measurement matrix (GRMM), while the random QPSK sequence achieves almost no gain. Furthermore, the numerical SIR performance follows the theoretical SIR for all three sequences. Figure 2 demonstrates the SIR performance obtained by averaging over 500 independent runs corresponding to independent interference waveforms, for different values of the maximum time delay \tilde{L} . We consider a case in which only one target exists and the jammer power is 225. One can see that a decrease in \tilde{L} can significantly improve SIR yielded by QPSK waveforms when \tilde{L} is less than 10. In contrast, Hadamard waveforms and rectangular pulse produce almost the same SIR for different values of \tilde{L} . This indicates that for QPSK waveforms the prior information of possible delays enables SIR improvement, while for the other two types of waveforms considered prior information did not make a difference.

2) *The CSM*: Figure 3 shows the histograms of the condition number and the maximum CSM using $\Phi_{\#2}$ for Hadamard waveforms and the GRMM produced in 100 random and independent runs. We consider the case of $M = 30$, $M_t = N_r = 10$ and the grid step of the discretized angle-range space is $[0.5^\circ, 15m]$. One can see that the numerical results fit the observations in Section III-B4, i.e., $\Phi_{\#2}$ increases the maximum CSM as compared to the GRMM with high probability. In Fig. 4 we use histograms to compare the CSM

corresponding to adjacent columns over 100 independent and random runs. Although $\Phi_{\#2}$ incorporates information about the waveforms, the distribution of the column correlation does not change significantly as compared to that of the conventional matrix. Among the three types of waveforms, the rectangular pulse gives rise to the worst CSM distribution, indicating that the performance of the proposed CS approach would be significantly degraded if rectangular pulses are transmitted. This is because the high autocorrelation of the rectangular pulse results in high CSM independently of the measurement matrix used.

B. The proposed measurement matrix $\Phi_{\#1}$

We consider a scenario in which $M_t = N_r = 4$ and three stationary targets exist. The azimuth angle and range of three targets are randomly generated in 100 runs within $[0^\circ, 1^\circ]$ and $[1000m, 1090m]$, respectively. The data of only one pulse is used and thus only the angle-range estimates can be obtained. The spacing of adjacent angle-range grid points is $[0.2^\circ, 15m]$. $\Phi_{\#1}$ is obtained from (14) based on the special structure of (17). Φ in (17) is replaced with $\Phi_{\#2}$. We consider different values of the tradeoff coefficient $\tilde{\lambda}$ in (14). Transmit nodes send Hadamard waveforms of length $L = 128$. Only $M = 20$ measurements per pulse are collected and forwarded to the fusion center by each node for CS-based MIMO radar while 100 measurements are used by the MIMO radar based on the matched filter method (MFM) [30].

Figure 5 shows the distribution of CSM for the GRMM, $\Phi_{\#1}$ and $\Phi_{\#2}$ in 100 random and independent runs. One can see that the GRMM and $\Phi_{\#2}$ lead to similar coherence distributions. $\Phi_{\#1}$ slightly reduces the maximum CSM and significantly increases the number of column pairs with low coherence as compared to the other two measurement matrices. $\Phi_{\#1}$ obtained from (16) using $\tilde{\lambda} = 0.6$ and $\tilde{\lambda} = 1.5$ produce a similar coherence distribution. Figure 6 shows the SIR performance of CS-based MIMO radar using the GRMM, $\Phi_{\#1}$ and $\Phi_{\#2}$, for different values of noise power in the absence of a jammer. One can see from Fig. 6 that $\Phi_{\#2}$ outperforms the other two measurement matrices in terms of SIR. $\Phi_{\#1}$ obtained from (16) using $\tilde{\lambda} = 0.6$ yields slightly better SIR than GRMM. As expected, increasing $\tilde{\lambda}$ from 0.6 to 1.5 moderately improves SIR.

Figures 7 and 8 compare the ROC performance of CS-based MIMO radar using the three aforementioned measurement matrices and MIMO radar based on the MFM, for different combinations of SNR and jammer-signal power. The probability of detection (PD) here denotes the percentage of cases in which all the targets are detected. The percentage of cases in which false targets are detected is denoted by the probability of false alarm (PFA). It is demonstrated in Figs. 7 and 8 that $\Phi_{\#1}$ and $\Phi_{\#2}$ with Hadamard waveforms can improve detection accuracy as compared to the GRMM in the case of mild and strong

interference, respectively. Since an increase in the tradeoff coefficient $\tilde{\lambda}$ can enhance SIR, $\Phi_{\#1}$ obtained from (16) using $\tilde{\lambda} = 1.5$ performs better in the case of strong interference than using $\tilde{\lambda} = 0.6$. Note that the three measurement matrices give rise to similar performance for $SNR = 10dB$ and $\beta = 0$. This is because the interference is sufficiently small so that all the measurement matrices perform well. Again, one can see that the MFM is inferior to the CS approach although it uses far more measurements than the CS approach.

It has been seen from Figs. 7 and 8 that the tradeoff coefficient $\tilde{\lambda}$ affects the performance of CS-based MIMO radar using $\Phi_{\#1}$. In order to further investigate the effect of $\tilde{\lambda}$, the curves of probability of detection accuracy are shown in Fig. 9 for $\tilde{\lambda} = 0.6, 1, 1.5, 2$ for different thresholds of hard detection. The probability of detection accuracy here denotes the percentage of cases in which no real targets are missing and no false targets exist. By taking all four combinations of SNR and jammer-signal power into account, $\tilde{\lambda} = 1.5$ results in the best performance. For a particular case, the optimal tradeoff coefficient depends on multiple factors, i.e., the basis matrix and the interference. The manner in which SIR and the CSM affect the support recovery of a sparse signal still remains unknown. Therefore, it is impossible to theoretically determine the optimal tradeoff coefficient.

V. CONCLUSIONS

We have proposed two measurement matrices in order to improve target detection performance of CS-based MIMO radar for the case in which the targets may be located across several range bins. The first one $\Phi_{\#1}$ aims at enhancing SIR and reducing the CSM at the same time. It is obtained by solving a convex optimization problem. This measurement matrix requires a heavy computational load as compared to the conventional measurement matrix, and also needs to adapt to a particular basis matrix. The computational burden of solving $\Phi_{\#1}$ can be alleviated through reducing the number of variables involved in the optimization problem. The second proposed measurement matrix $\Phi_{\#2}$ targets improving SIR only. It is constructed based on the transmit waveforms and also accounts for all possible discretized delays of target returns within the given time window. $\Phi_{\#2}$ is dependent on the range grid only and requires much lower complexity than does $\Phi_{\#1}$. It is shown that $\Phi_{\#2}$ based on reduced bandwidth transmit waveforms can improve SIR, but on the other hand, using waveforms that are too narrowband increases the CSM, thus invalidating conditions for the application of the CS approach. Therefore, the waveforms must be chosen carefully to guarantee the desired performance using the second measurement matrix. Numerical results show that $\Phi_{\#1}$ and $\Phi_{\#2}$ with the proper waveforms (e.g., Hadamard codes) can improve detection accuracy as compared to the Gaussian random measurement matrix in the case of

small and strong interference, respectively.

Acknowledgment

The authors would like to thank Dr. Rabinder Madan of the Office of Naval Research for sharing his ideas on the use of compressive sampling in the context of MIMO radar.

REFERENCES

- [1] E. Fishler, A. Haimovich, R. Blum, D. Chizhik, L. Cimini and R. Valenzuela, "MIMO radar: An idea whose time has come," in *Proc. IEEE Radar Conf.*, Philadelphia, PA, pp. 71-78, Apr. 2004.
- [2] L. Xu, J. Li and P. Stoica, "Radar imaging via adaptive MIMO techniques," in *Proc. European Signal Process. Conf.*, Florence, Italy, Sep. 2006.
- [3] J. Li, P. Stoica, L. Xu and W. Roberts, "On parameter identifiability of MIMO radar," *IEEE Signal Process. Lett.*, vol. 14, no. 12, pp. 968-971, Dec. 2007.
- [4] A.M. Haimovich, R.S. Blum and L.J. Cimini, "MIMO radar with widely separated antennas," *IEEE Signal Process. Magazine*, vol. 25, no. 1, pp. 116-129, Jan. 2008.
- [5] H. Godrich, A.M. Haimovich, and R.S. Blum, "Target localization accuracy gain in MIMO radar based system," *IEEE Trans. Info. Theory*, vol.56, no.6, pp.1-21, Jun. 2010.
- [6] Q. He, R.S. Blum, H. Godrich, and A.M. Haimovich, "Target velocity estimation and antenna placement for MIMO radar with widely separated antennas", *IEEE Journal of Selected Topics in Signal Process.*, vol. 4, no. 1, pp. 79-100, Feb. 2010.
- [7] P. Stoica and J. Li, "MIMO radar with colocated antennas," *IEEE Signal Process. Magazine*, vol. 24, no. 5, pp. 106-114, Sep. 2007.
- [8] C. Chen and P.P. Vaidyanathan, "MIMO radar space-time adaptive processing using prolate spheroidal wave functions," *IEEE Trans. Signal Process.*, vol. 56, no. 2, pp. 623-635, Feb. 2008.
- [9] D.V. Donoho, "Compressed sensing," *IEEE Trans. Info. Theory*, vol. 52, no. 4, pp. 1289-1306, Apr. 2006.
- [10] E.J. Candes, "Compressive sampling," in *Proc. The Int'l Congress of Mathematicians*, Madrid, Spain, pp. 1433-1452, Aug. 2006.
- [11] E.J. Candes and M.B. Wakin, "An introduction to compressive sampling [A sensing/sampling paradigm that goes against the common knowledge in data acquisition]," *IEEE Signal Process. Magazine*, vol. 25, no. 2, pp. 21-30, Mar. 2008.
- [12] J. Romberg, "Imaging via compressive sampling [Introduction to compressive sampling and recovery via convex programming]," *IEEE Signal Process. Magazine*, vol. 25, no. 2, pp. 14-20, Mar. 2008.
- [13] E.J. Candes, J.K. Romberg and T. Tao, "Stable signal recovery from incomplete and inaccurate measurements," *Communications on Pure and Applied Mathematics*, vol. 59, no. 8, pp. 1207-1223, Aug. 2006.
- [14] R. Baraniuk and P. Steeghs, "Compressive radar imaging," in *Proc. IEEE Radar Conf.*, Boston, MA, pp. 128-133, Apr. 2007.
- [15] A.C. Gurbuz, J.H. McClellan and W.R. Scott, "Compressive sensing for GPR imaging," in *Proc. 41th Asilomar Conf. Signals, Syst. Comput.*, Pacific Grove, CA, pp. 2223-2227, Nov. 2007.
- [16] M.A. Herman and T. Strohmer, "High-resolution radar via compressed sensing," *IEEE Trans. Signal Process.*, vol. 57, no. 6, pp. 2275-2284, Jun. 2009.

- [17] M. Herman and T. Strohmer, "Compressed sensing radar," in *Proc. IEEE Int'l Conf. Acoust. Speech Signal Process*, Las Vegas, NV, pp. 2617-2620, Mar.-Apr. 2008.
- [18] A.P. Petropulu, Y. Yu and H.V. Poor, "Distributed MIMO radar using compressive sampling," in *Proc. 42nd Asilomar Conf. Signals, Syst. Comput.*, Pacific Grove, CA, pp. 203-207, Nov. 2008.
- [19] C.Y. Chen and P.P. Vaidyanathan, "Compressed sensing in MIMO radar," in *Proc. 42nd Asilomar Conf. Signals, Syst. Comput.*, Pacific Grove, CA, pp. 41-44, Nov. 2008.
- [20] T. Strohmer and B. Friedlander, "Compressed sensing for MIMO radar - algorithms and performance," in *Proc. 43rd Asilomar Conf. Signals, Syst. Comput.*, Pacific Grove, CA, pp. 464-468, Nov. 2009.
- [21] Y. Yu, A.P. Petropulu and H.V. Poor, "MIMO radar using compressive sampling," *IEEE Journal of Selected Topics in Signal Process.*, vol. 4, no. 1, pp. 146-163, Feb. 2010.
- [22] Y. Yu, A.P. Petropulu and H.V. Poor, "CSSF MIMO radar: Low-complexity compressive sensing based MIMO radar that uses step frequency," submitted to *IEEE Trans. Aerospace and Electronic Sys.*.
- [23] E.J. Candes and T. Tao, "The Dantzig selector: Statistical estimation when p is much larger than n ," *Ann. Statist.*, vol. 35, no. 6, pp. 2313-2351, Dec. 2007.
- [24] W. Dai and O. Milenkovic, "Subspace pursuit for compressive sensing signal reconstruction," *IEEE Trans. Info. Theory*, vol. 55, no. 5, pp. 2230-2249, May 2009.
- [25] D. Needell and J. Tropp, "CoSaMP: Iterative signal recovery from incomplete and inaccurate samples," *Appl. Comput. Harmonic Anal.*, vol. 26, no. 3, pp. 301-321, May 2009.
- [26] G. Tang and A. Nehorai, "Performance analysis for sparse support recovery," *IEEE Trans. Info. Theory*, vol. 56, no. 3, pp. 1383-1399, Mar. 2009.
- [27] J.A. Tropp, "Greed is good: Algorithmic results for sparse approximation," *IEEE Trans. Info. Theory*, vol. 50, no. 10, pp. 2231-2242, Oct. 2004.
- [28] J.A. Tropp, "Just relax: Convex programming methods for identifying sparse signals," *IEEE Trans. Info. Theory*, vol. 55, no. 2, pp. 917-918, Feb. 2009.
- [29] H. Ochiai, P. Mitran, H.V. Poor and V. Tarokh, "Collaborative beamforming for distributed wireless ad hoc sensor networks," *IEEE Trans. Signal Process.*, vol. 53, no. 11, pp. 4110-4124, Nov. 2005.
- [30] N. Levanon and E. Mozeson, *Radar Signals*, Hoboken, NJ: J. Wiley, 2004.

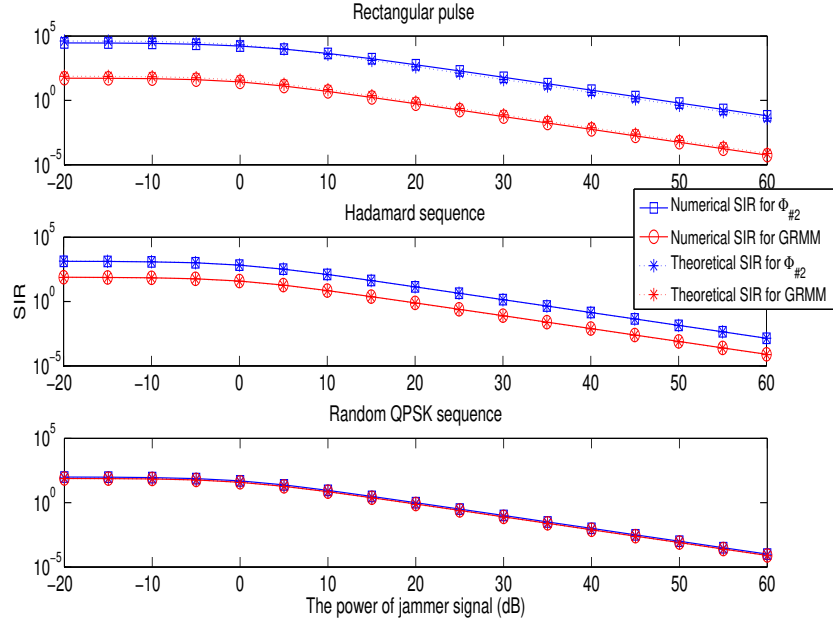


Fig. 1. SIR corresponding to GRMM and $\Phi_{\#2}$ for different transmit waveforms ($M = M_t = 30$ and $N_r = 1$).

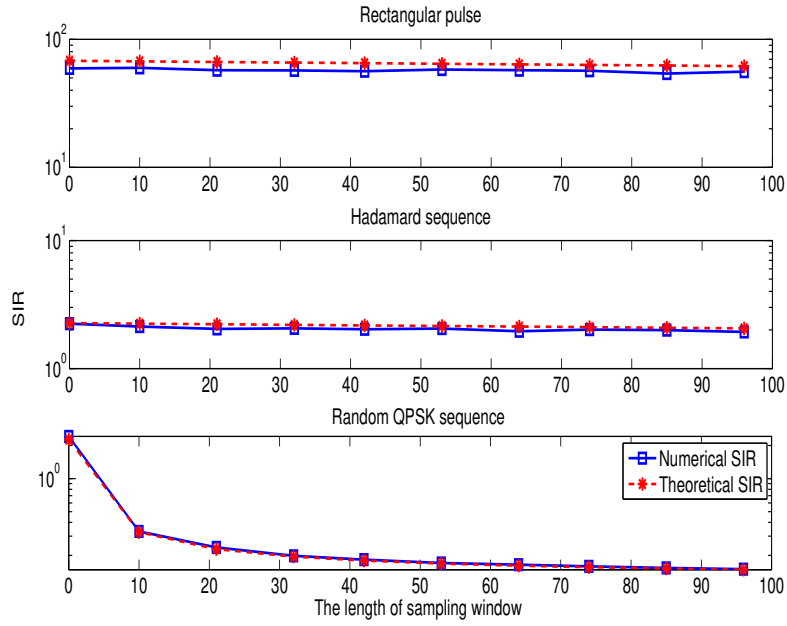


Fig. 2. SIR corresponding to $\Phi_{\#2}$ for different values of \tilde{L} ($M = M_t = 30$ and $N_r = 1$).

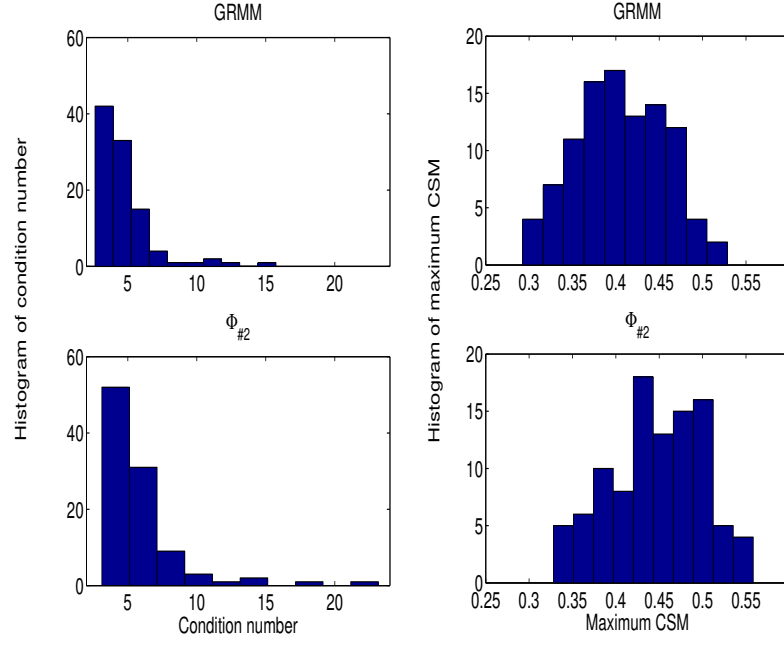


Fig. 3. Conditional number and the maximum coherence of the sensing matrix based on $\Phi_{\#2}$ ($M = 30$ and $N_r = M_t = 10$).

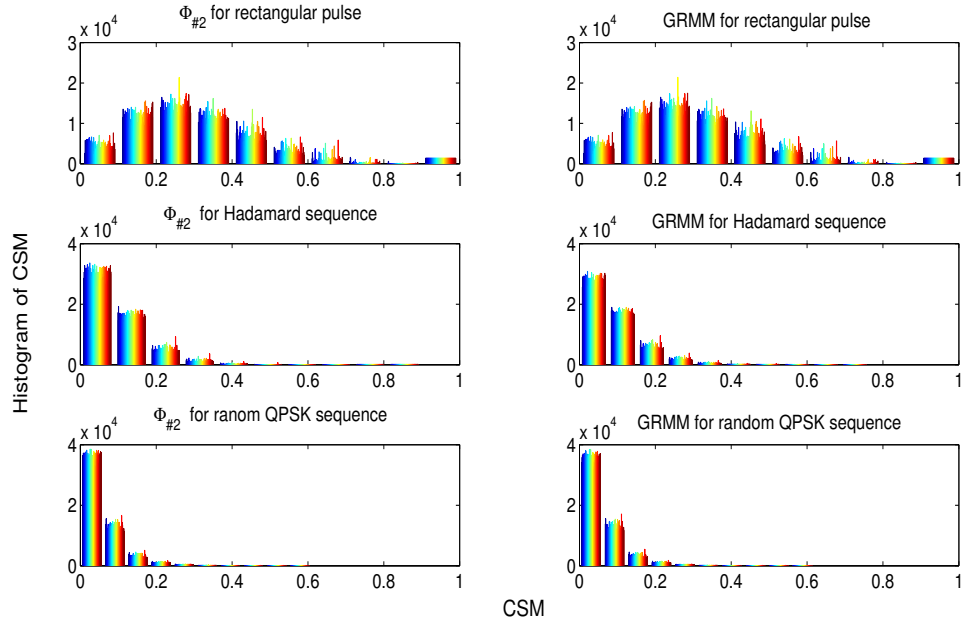


Fig. 4. Coherence of adjacent columns of the sensing matrix based on $\Phi_{\#2}$ for different transmit sequences ($M = 30$ and $M_t = N_r = 10$).

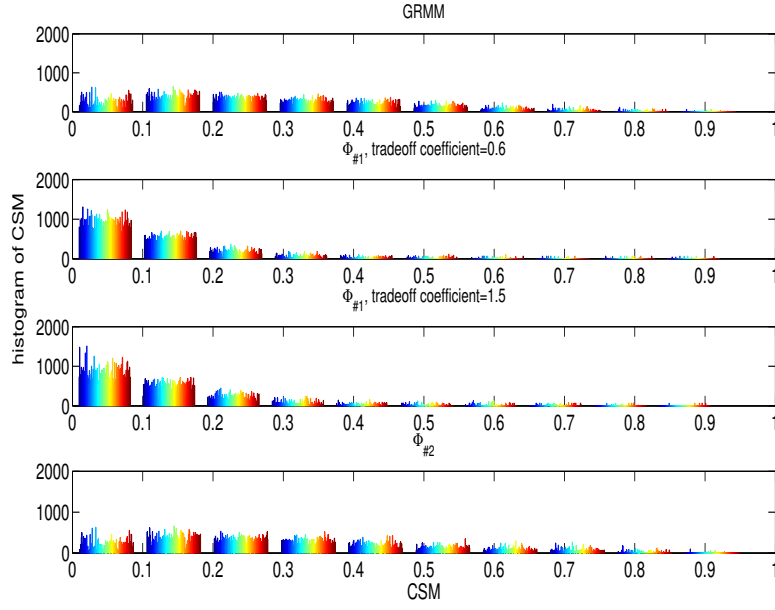


Fig. 5. Coherence distribution of cross columns of the sensing matrix using $\Phi_{\#1}$, $\Phi_{\#2}$ and the GRMM ($M_t = N_r = 4$).

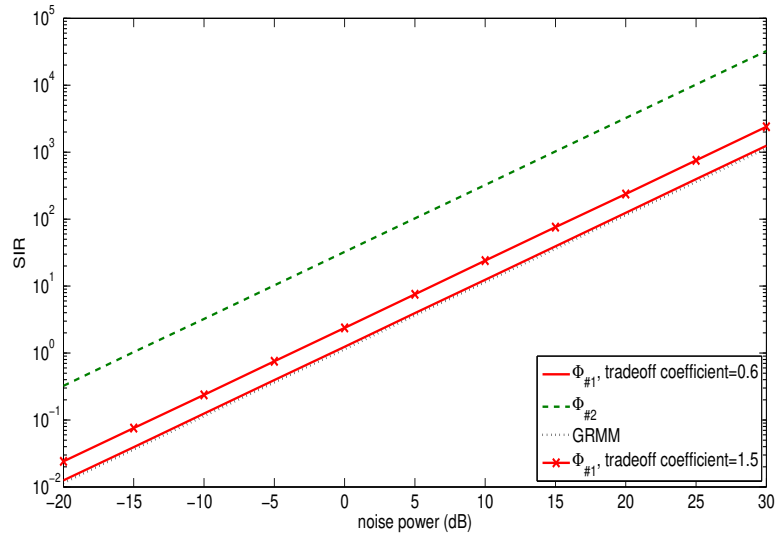


Fig. 6. SIR for CS-based MIMO radar using $\Phi_{\#1}$, $\Phi_{\#2}$ and GRMM for different values of noise power ($M_t = N_r = 4$).

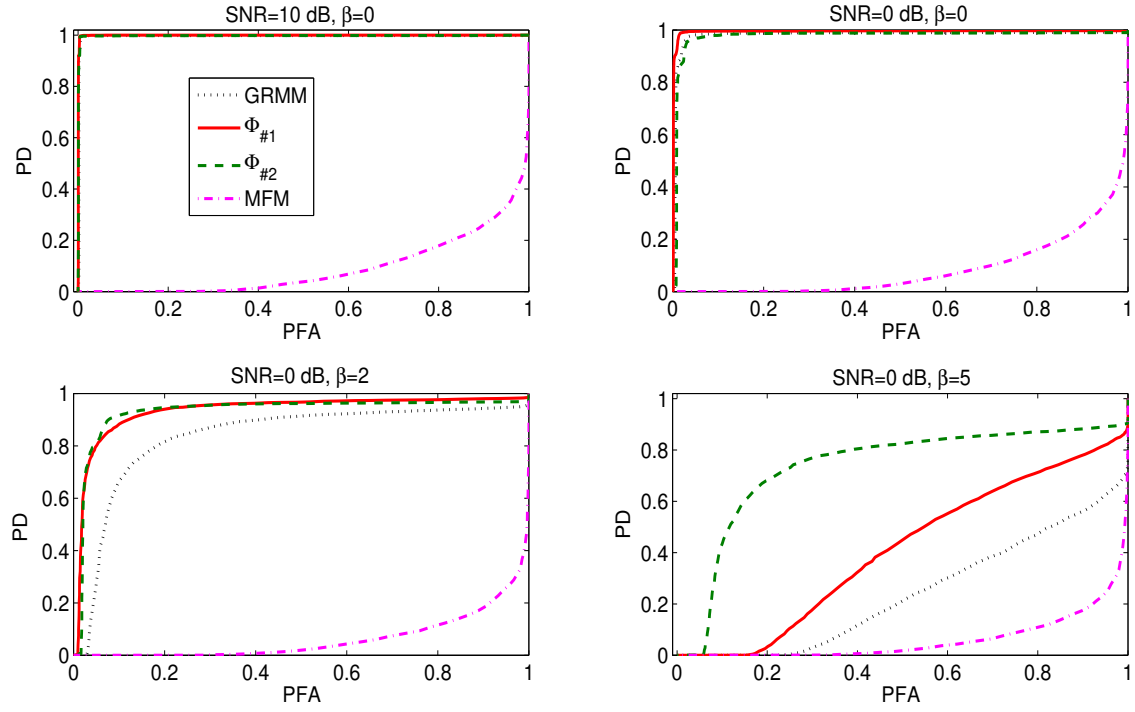


Fig. 7. ROC curves for CS-based MIMO radar using $\Phi_{\#1}$, $\Phi_{\#2}$ and the GRMM and for MIMO radar using the MFM ($M_t = N_r = 4$ and $\tilde{\lambda} = 0.6$).

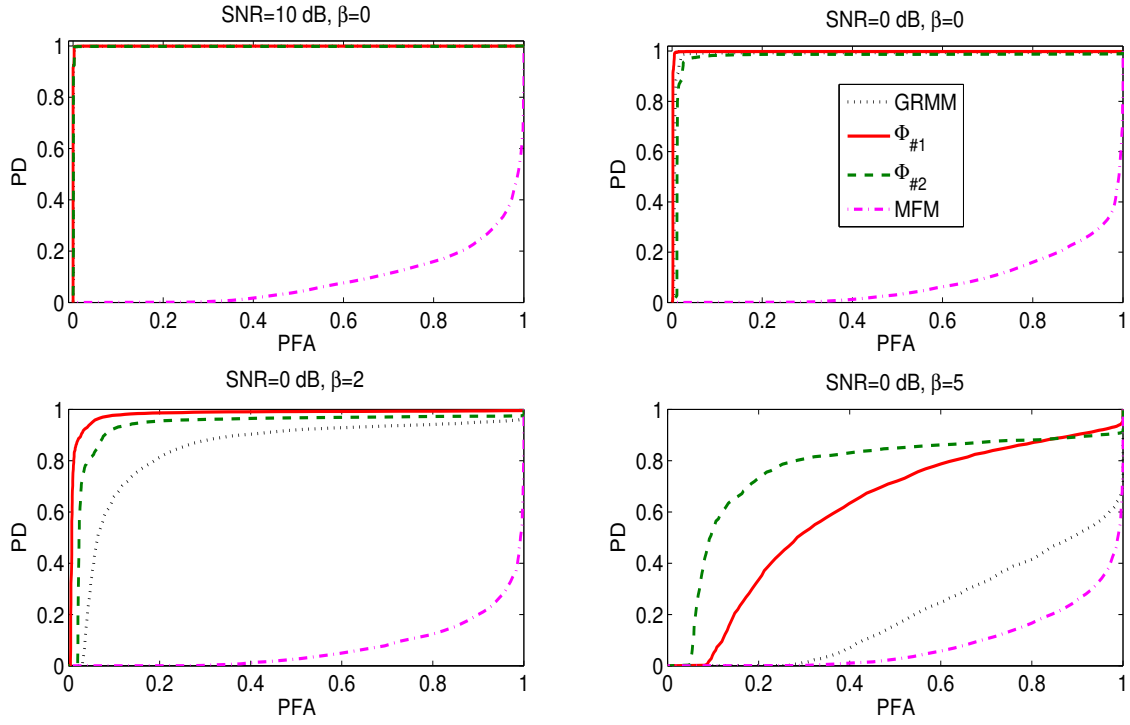


Fig. 8. ROC curves for CS-based MIMO radar using $\Phi_{\#1}$, $\Phi_{\#2}$ and the GRMM and for MIMO radar using the MFM ($M_t = N_r = 4$ and $\tilde{\lambda} = 1.5$).

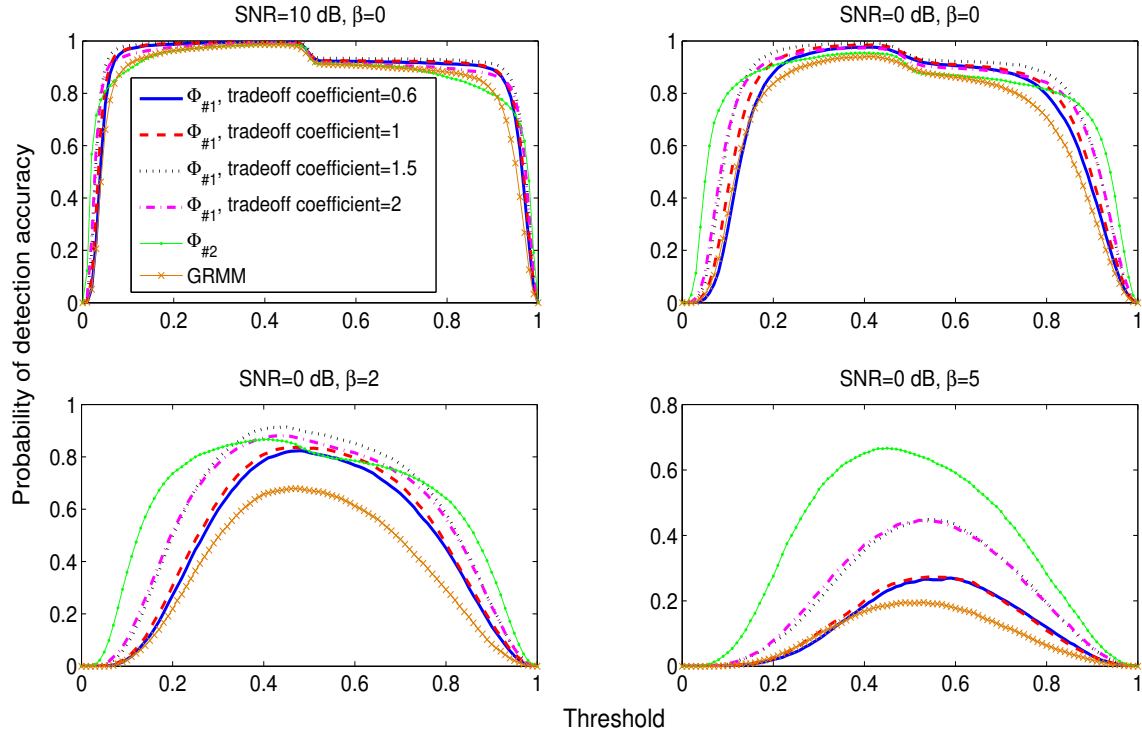


Fig. 9. The probability of detection accuracy for CS-based MIMO radar using $\Phi_{\#1}$, $\Phi_{\#2}$ and the GRMM for different values of $\tilde{\lambda}$ ($M_t = N_r = 4$).